Progress In Electromagnetics Research M, Vol. 116, 145–154, 2023

A Triband Hexagonal Shaped Polarization Insensitive Absorber by Tuning Graphene Material in Terahertz Frequency Domain

Nagandla Prasad[1], Pokkunuri Pardhasaradhi[1], Boddapati T. P. Madhav[1, *], Vysyaraju L. Raju[2], and Pucha P. Priya[3]

Abstract—Terahertz era is becoming a more prominent and expanding platform for a variety of applications. In this paper, we propose a triband absorber with a hexagon-shaped radiating patch for THz applications. The proposed structure has three layers: a hexagonal patch made of graphene as a radiating patch, a silicon layer as a dielectric substrate, and a bottom conductive layer made of gold to prevent EM wave transmission. The proposed structure operates at three resonant frequencies 0.38 THz, 1.23 THz, and 1.77 THz, respectively. We may accomplish maximum absorption level (above 90%) and maximum absorption bandwidth by setting relevant chemical potential and relaxation times to 0.2 ev and 0.2 ps, respectively. The proposed structure contains a lossy silicon substrate, which has a dielectric constant of 11.9 and a loss tangent of 2.5e−004. The proposed structure is experimented with three layers, and the effect on absorbance for different modes is illustrated.

1. INTRODUCTION

Terahertz frequency ranging from 0.1 THz to 10 THz is named terahertz era or terahertz gap [1, 2]. Because of the rising demand for higher data rates, the terahertz frequency domain has become an attraction for researchers all over the world. The metamaterial is a buzzword in the market for the past few decades, because of its applications in the field of electromagnetics. Metamaterial is an artificially engineered structure, whose operating wavelength is less than visible light. First, in 2008, the metamaterial absorber was proposed by Landy et al. [3], and later many articles came on metamaterial-based absorbers. Metamaterial based structures contain many extraordinary properties compared to normal conventionally available materials, like a negative refractive index (either μ or ε is negative [4], or both may be negative [5]) and electromagnetic wave absorption [6, 7]. If the electrical permittivity (ε) and magnetic permeability (μ) both are negative, then metamaterials are named as double-negative (DNG) materials. Because of the mentioned properties, the metamaterials can be used in many applications like filters [8], shielding [9], cloaking devices [10], super lens [11], beam tilting [12], terahertz communications [13], improving the performance of an antenna. Metamaterial absorber contains many advantages like selecting the desired frequency band, having a small size, and having less weight. The problem with the metasurface absorber is that once it has been constructed, it gives some response based on the size and shape of the structure, and there is no additional tunability with the structure. This problem can be mitigated by using micro-electromechanical systems (MEMSs) [14] and electronic tuning components [15], but the main drawbacks of these methods are high cost and high fabrication complexity. Therefore, to overcome these problems there is a necessity to introduce new materials for the design process. For the last decade, graphene material plays a key role in designing

Received 15 March 2023, Accepted 18 April 2023, Scheduled 30 April 2023
* Corresponding author: Boddapati Taraka Phani Phaneendra Madhav (btpmadhav@kluniversity.in).
[1] Antennas and Liquid Crystals Research Center, Department of ECE, Koneru Lakshmaiah Education Foundation, Vaddeswaram, Guntur, Andhra Pradesh, India. [2] Department of ECE, Aditya Institute of Technology and Management, Tekkali, India.
[3] Department of ECE, Dadi Institute of Engineering and Technology, Anakapalle, India.

terahertz devices. Graphene material is different from the remaining materials as it contains a single-layered structure which is formed by carbon atoms and arranged like a honeycomb structure. Graphene has many advantages as it is more flexible than the remaining materials, compact in size, lightweight, and strong. Additionally, for both infrared and THz frequency regions, graphene material allows surface plasmon resonance [16]. Graphene conductivity can be altered by tuning its chemical potential. There are numerous articles produced based on metasurface absorbers by tuning graphene material. Jain et al. [17] proposed a graphene metasurface based polarization-insensitive quadband absorber for terahertz applications with a unit cell size of $48.2 * 48.2\,\mu m^2$. A graphene material-based square-type split ring resonator (SRR) is proposed by Asgari and Fabritius [18], for multi-band applications with a unit cell size of $20 * 20\ \mu m^2$. Another polarization-insensitive broadband terahertz absorber is proposed by Feng et al. [19], with $73 * 73\,\mu m^2$ size, and graphene material is used as a radiating patch with a circular ring and a cross shape. A multi-layered metasurface absorber is proposed by Huang [20] et al. for polarization-insensitive broadband applications. Nejat and Nozhat [21] proposed a cross-shaped absorber using graphene material for polarization-insensitive broadband applications in the terahertz domain with $80 * 80\,\mu m^2$.

There are many materials available to change the performance of a metasurface, such as V02, liquid crystals, and graphene. Graphene is the most favored material among all existing materials since it is a carbon nanomaterial that is laid out in a honeycomb lattice pattern and has amazing qualities such as optical, thermal, and mechanical ones. Graphene is the toughest substance known to man, softer than rubber, and more elastic than diamond, with greater electron mobility than silicon and greater conductivity than copper. Not only is graphene thin, but it is also extremely transparent to visible light and has surface plasmon resonance at terahertz frequencies. The performance of any metasurface can be adjusted at terahertz frequencies by altering the chemical potential of graphene material. Because of its numerous advantages, we picked graphene as a radiating patch. In this article, we present a graphene-based metasurface absorber for terahertz applications.

2. PROPOSED STRUCTURE DESCRIPTION

2.1. Unit Cell Design Procedure

Numerical simulation tools like CSTMW studio, which is based on the finite-difference time-domain (FDTD) method, were used to simulate the proposed unit cell structure. As shown in Figure 1, the proposed unit cell structure contains three layers. To prevent the transmission of electromagnetic (EM) waves, the bottom layer is made of conducting material like gold (Au) with a thickness of 0.5 μm. The electric conductivity of gold is chosen as 4.561e+007 s/m, and the overall size of the gold layer is $70 * 70 * 0.5\,\mu m^3$. The top layer of the proposed unit cell structure contains a hexagonal graphene patch with a thickness of 0.1 μm. A lossy silicon dielectric material is sandwiched between the top and bottom

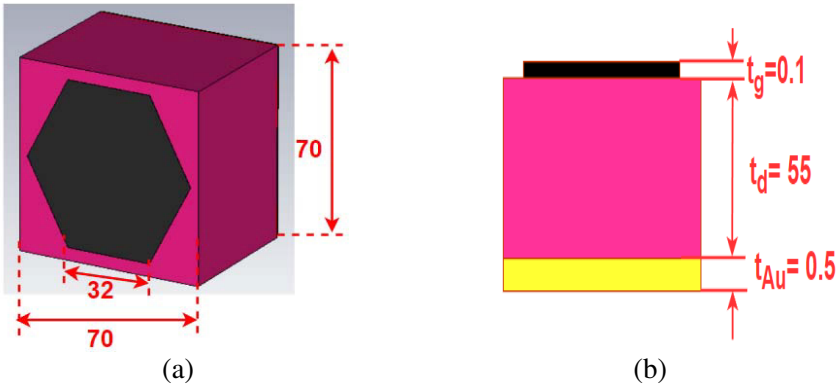

Figure 1. Proposed unit cell structure with dimentions (All are in μm), (a) unit cell's prospective view, (b) side view of unit cell.

layers. Here, the thickness of the dielectric material is chosen as 55 µm, and the dielectric constant is chosen as 11.9 with a loss tangent of 2.5e−004. The initial choice for the chemical potential, relaxation time, and temperature of the graphene-based unit cell is 1 eV, 0.1 ps, and 300°k, respectively. Kubo formulae [22] is used to calculate the surface conductivity of graphene material.

The simulation can be performed by using an FDTD-based tool like CSTMW Studio, which can be employed in electromagnetic problem-solving that demands exact and speedy replies. The main notable advantage of the CST tool is that the resource needs to scale only linearly according to the number of mesh nodes. As a result, massive radiating structures can be handled easily and quickly. While performing the simulation, we choose a frequency-domain solver for getting an oblique incidence response for the absorber rather than normal incidence which is possible by the time-domain solver in CST. The FD solver is a strong 3D full-wave solver with exceptional computing effectiveness. While simulation is performed, frequency is selected initially, and perfect electric and magnetic boundary conditions are applied along the x- and y-directions to impinge the EM wave in the z-direction as shown in Figure 2.

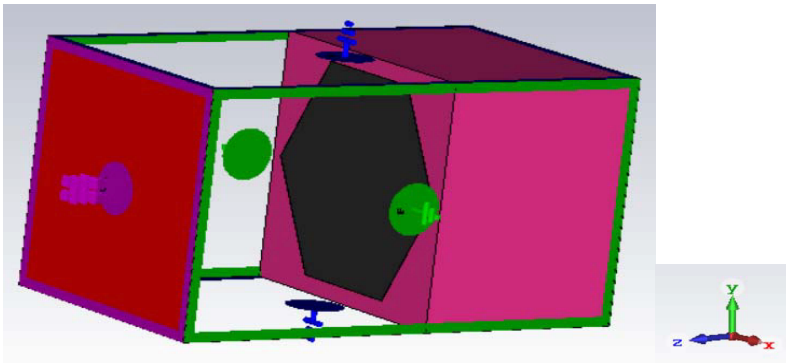

Figure 2. Simulation setup for the proposed unit cell structure.

2.2. General Discussion of a Graphene Based Absorber and Proposed Structure

The concept of EM wave absorption can be explained by using transmission line theory. To achieve complete EM wave absorption, the metamaterial impedance must match the EM wave impedance, so that the metasurface does not reflect EM waves.

The following formula can be utilized to calculate the absorption of a metasurface. Generally, the absorption of a metasurface absorber can be represented in terms of scattering parameters as the following formula.

$$\text{Absorption (A)} = 1 - |S_{11}^2| - |S_{21}^2| \tag{1}$$

From the equation, we can say that A represents the absorption, $|S_{11}^2|$ the reflection coefficient, and $|S_{21}^2|$ the transmission coefficient of an absorber. Because the bottom layer of the proposed absorber is a perfect conducting material like gold, the transmission coefficient is almost zero (i.e., $|S_{21}^2| = 0$) for the metasurface absorber. Eq. (1) can be reformulated as follows.

$$\text{Absorption (A)} = 1 - |S_{11}^2| \tag{2}$$

Kubo [18, 23] calculated formulae for the surface conductivity of a graphene material which are realized by the following equations.

$$\sigma(\omega) = \sigma_{\text{inter}}(\omega) + \sigma_{\text{intra}}(\omega) \tag{3}$$

$$\sigma_{\text{intra}}(\omega) = \frac{-je^2K_BT}{\Pi h^2(\omega - j\Gamma)}\left\{\frac{\mu_c}{K_BT} + 2 * \ln\left[\exp\left(\frac{-\mu_c}{K_BT}\right) + 1\right]\right\} \tag{4}$$

$$\sigma_{\text{inter}}(\omega) = \frac{-je^2}{4\Pi h}\left\{\ln\left[\exp\left(\frac{2\mu_c - (\omega - j\Gamma)h}{2\mu_c + (\omega - j\Gamma)h}\right)\right]\right\} \tag{5}$$

$$\Gamma = \frac{eV_F^2}{\mu_c \mu} \tag{6}$$

In addition, in the terahertz frequency domain, the chemical voltage is much larger than the product of Boltzmann's constant and kelvin temperature. Consequently, Eq. (3) can be changed as

$$\sigma_{\text{intra}}(\omega) = \frac{-je^2 K_B T}{\Pi h^2(\omega - j\Gamma)} \left(\frac{\mu_c}{K_B T} + 0 \right) = \frac{-je^2 \mu_c}{\Pi h^2(\omega - j\Gamma)} \tag{7}$$

Here, $\sigma_{\text{inter}}(\omega)$ represents the inter-band conductivity due to the electron-hole pair generation and recombination, and $\sigma_{\text{intra}}(\omega)$ is the intra-band conductivity due to free charge carriers. $\hbar * 2\Pi = h$ is the reduced Plank's constant, ω the angular frequency, Γ the scattering rate ($\Gamma = 1/2\tau$) where τ is the relaxation time, e the charge of an electron, V_F the Fermi velocity of 10^6 meters/seconds, K_B the Boltzmann's constant, μ_c the chemical potential of graphene material which is varied from 0 eV to 0.3 eV, and T the temperature measured in kelvins. From Figure 4, we can note that the proposed structure resonates at three different resonant frequencies, 0.38 THz, 1.23 THz, and 1.77 THz. Here, the green colour indicates the reflection spectrum for $3 * 3$ array. Finally, we can conclude that for any array size of the proposed unit cell structure, the percent level of absorption is almost same. Here, we consider $3 * 3$ array sized metasurface, as shown in Figure 3, by fixing chemical potential as 0.2 eV and relaxation time as 0.1 ps at 300°k.

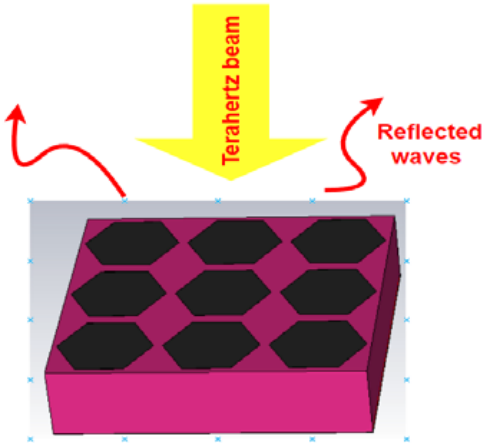

Figure 3. Proposed absorber with 3×3 array size.

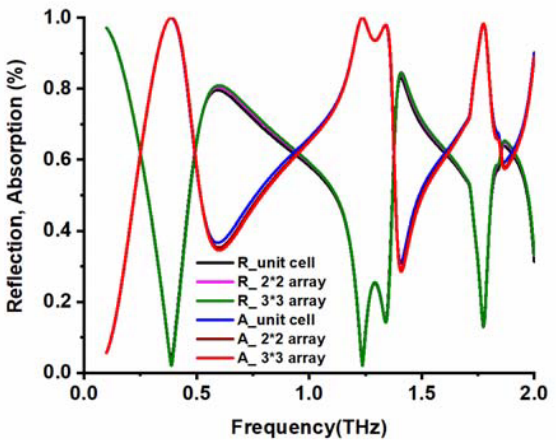

Figure 4. Absorption (A), Reflection (R) for different array sized unit cell.

3. RESULTS AND ANALYSIS

The graphene's relaxation time (τ) plays an important role in controlling absorption bandwidth and the absorption level of a metasurface absorber. From Figure 5, it can be noted that the frequency and percent level of absorption are selected on the x- and y-axes, respectively, and the frequency limit is chosen from 0.1 THz to 2 THz. Here, the black colored curve represents the percent level absorption spectrum of 0.1 ps; the red colored curve represents the percent level absorption spectrum of 0.2 ps; and finally, the blue colored curve represents the percent level absorption spectrum of 0.3 ps. Figure 6 indicates a contour plot for the variation of different relaxation time (τ) parameters. From Figure 5, we can realize that at 0.1 ps, the percent level of absorption, which is indicated with red color, is low at 0.386 THz frequency. At 0.2 ps, the absorption bandwidth is more than that at 0.1 ps, and further at 0.3 ps the absorption bandwidth is split into two portions at 1.23 THz frequency. From the three relaxation times, we have chosen 0.2 ps as a better relaxation time, since good absorption bandwidth and good absorption level (above 90 percent) are achieved at this relaxation time. Another important parameter of graphene material for controlling the absorption bandwidth and absorption level of a metasurface absorber is chemical potential (μ_c). The variation of the percent level of absorption and

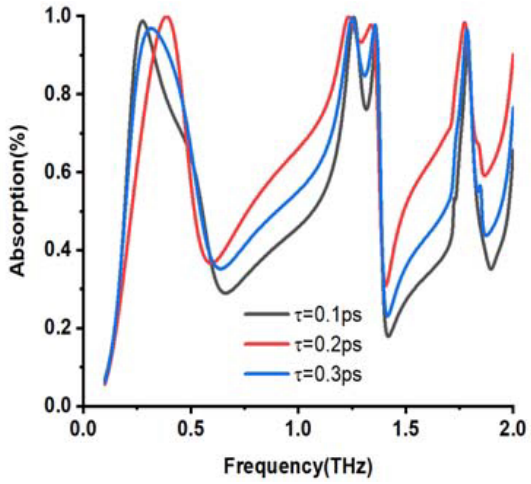

Figure 5. Absorption spectra for variation of relaxation time (τ).

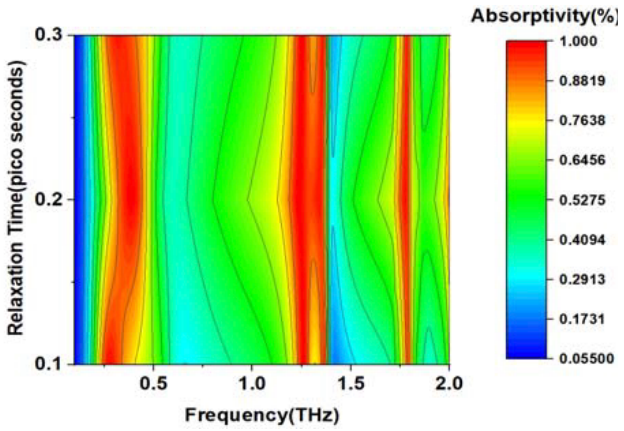

Figure 6. Contour plot for relaxation time (τ) variation.

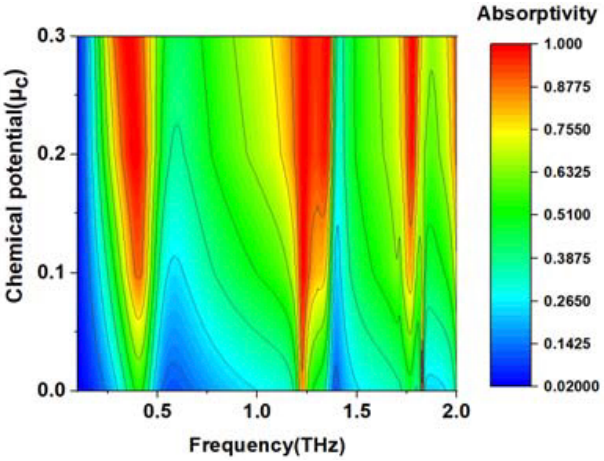

Figure 7. Contour plot for the variation of chemical potential (μ_c).

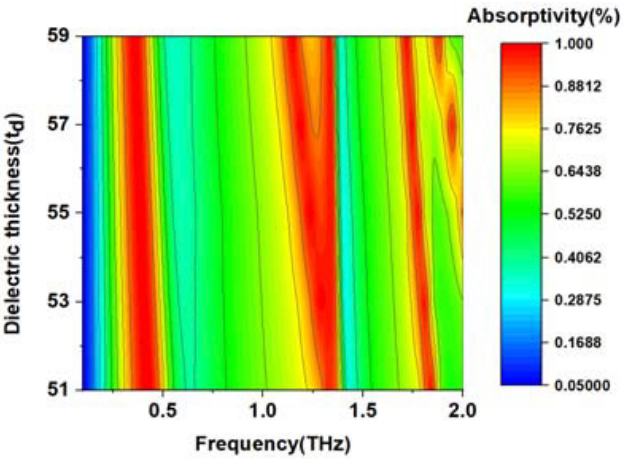

Figure 8. Contour plot for variation of lossy silicon dielectric material thickness (d).

absorption bandwidth of the proposed absorber is shown in Figure 7. From Figure 7, we can note that the frequency and chemical potential of graphene material are chosen along x- and y-directions, respectively. From Figure 6, we can realize that before applying a chemical potential ($\mu_c = 0\,\text{eV}$), the percent level of absorption is very poor at three resonant frequencies, 0.386 THz, 1.23 THz, and 1.77 THz. At $\mu_c = 0.1\,\text{eV}$, the absorption bandwidth which is above 90 percent level increases slowly, and at $\mu_c = 0.2\,\text{eV}$, we achieve maximum absorption bandwidth for three resonating frequency bands 0.32 THz to 0.43 THz, 1.19 THz to 1.35 THz, and 1.74 THz to 1.79 THz, respectively. The performance of the structure for different dielectric thickness values can be achieved by applying a parametric analysis for the substrate thickness parameter in the CST simulator and selecting a range from 51 μm to 59 μm with a step size of 2 μm, then the response of the structure is shown in Figure 8. From Figure 8, it is shown that the frequency and dielectric material thickness parameters are selected on the x- and y-axes, respectively, and the frequency limit is chosen from 0.1 THz to 2 THz. We can note that for the first resonating band, the absorption bandwidth is constant from 0.32 THz to 0.43 THz frequency. For the second band, the absorption bandwidth is less at 51 μm, and at 55 μm, the absorption bandwidth is split into 2 parts. So to have constant maximum bandwidth we have chosen dielectric material thickness as 55 μm. Finally, for the third resonant frequency band, the absorption bandwidth is constant.

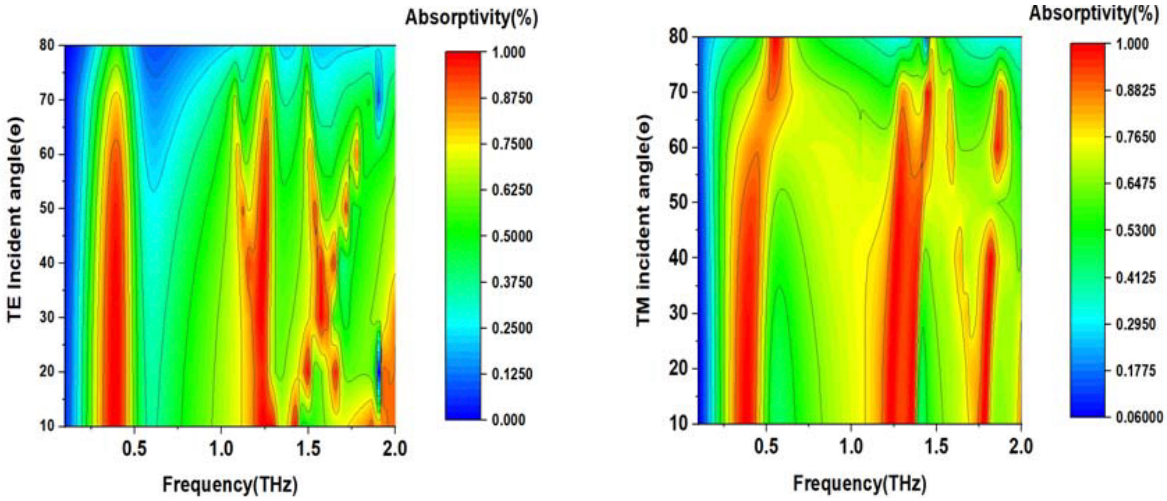

Figure 9. At chemical potential (μ_c) = 0.2 eV and relaxation time (τ) = 0.2 ps, the proposed structure's absorption contour map as a function of frequency and different oblique incidence angles (θ) for (a) TE mode and (b) TM mode.

The effect of various oblique incident angles (θ) on absorption bandwidth is shown in Figure 9, for both TE and TM modes. From Figure 9(a), we can note that for the TE mode of the proposed structure, the absorption bandwidth (> 90 percent absorption level) for the first resonating band (0.32 THz to 0.43 THz) is constant up to 50-degree incident angle, and around 60-degree angle, the absorption bandwidth, indicated by red color, has vanished. For the second resonant frequency band (1.74 THz–1.79 THz), the absorption is constant up to a 65-degree incident angle, and for the third resonant frequency band (1.19 THz to 1.35 THz), the absorption bandwidth is constant for 25 to 40 degrees. Similarly, for the TM mode of operation, the first absorption bandwidth is constant up to 50 degrees; around 60-degree angle; the absorption level is low; the bandwidth is bent with lower absorption; and finally, the absorption bandwidth is reduced. For the second band, the absorption bandwidth is constant up to a 55-degree incident angle; later the spectrum is split into two portions; and finally, the absorption has vanished around a 70-degree incident angle. Similarly, for the third band, the absorption bandwidth is constant up to 40 degrees; at a 50-degree incident angle, a lower absorption level is observed later around a 70-degree angle; and the absorption has vanished. Figure 10(a) represents the absorption spectrum for different polarization angles, and Figure 10(b) represents the contour plot for the TE mode of operation. From Figure 10, we can note that for polarization angles up to 80 degrees, the absorption bandwidth is constant in the TE mode of operation. Figure 11 represents the absorption plot for different polarization angles under TM mode. Except at a 70-degree polarized angle, for the third frequency resonating band under TM mode, for all the remaining frequency bands and remaining polarization angles, a constant absorption bandwidth is observed.

From Figure 12(a), we can note that at 0.386 THz frequency, a small amount of electric field which is indicated with red color is formed at the corners of the hexagonal graphene patch. For 1.23 THz frequency, more electric field is formed like folded bracket shape on graphene hexagonal patch edges, and at 1.77 THz frequency, which is indicated in Figure 12(c), a strong electric field is formed in silicon dielectric substrate material like cylinder shape and on the graphene patch. From Figure 13(a), we can note that a strong magnetic field is present in silicon and gold material, and in Figure 13(c), the field almost occupies all the edges of the hexagonal graphene patch. From Figure 12 and Figure 13, we can realize that a good agreement exists between electric and magnetic fields as they are perpendicular to each other. From Figure 14, we can note that the maximum current is observed on the horizontal edges of the hexagonal patch at 0.386 THz frequency. A small amount of current is observed at the center of the graphene patch, and some maximum current is observed at 1.23 THz frequency. The total exterior part of the hexagonal graphene patch is covered with maximum current at 1.77 THz frequency. Table 1 shows

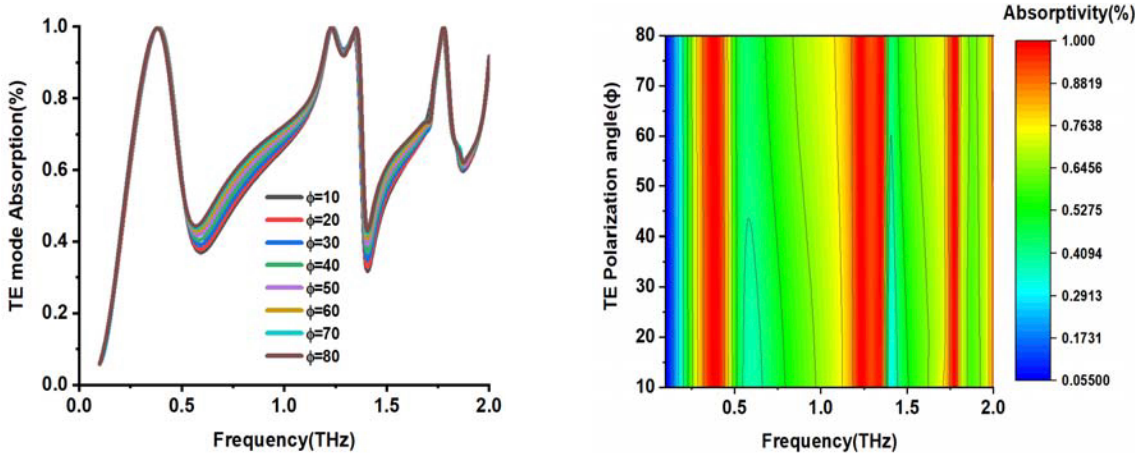

(a) (b)

Figure 10. At chemical potential (μ_c) = 0.2 eV and relaxation time (τ) = 0.2 ps, the proposed structure's absorption contour map as a function of frequency and different polarization angles (ϕ) in TE mode with (a) absorption level spectrum, (b) contour map.

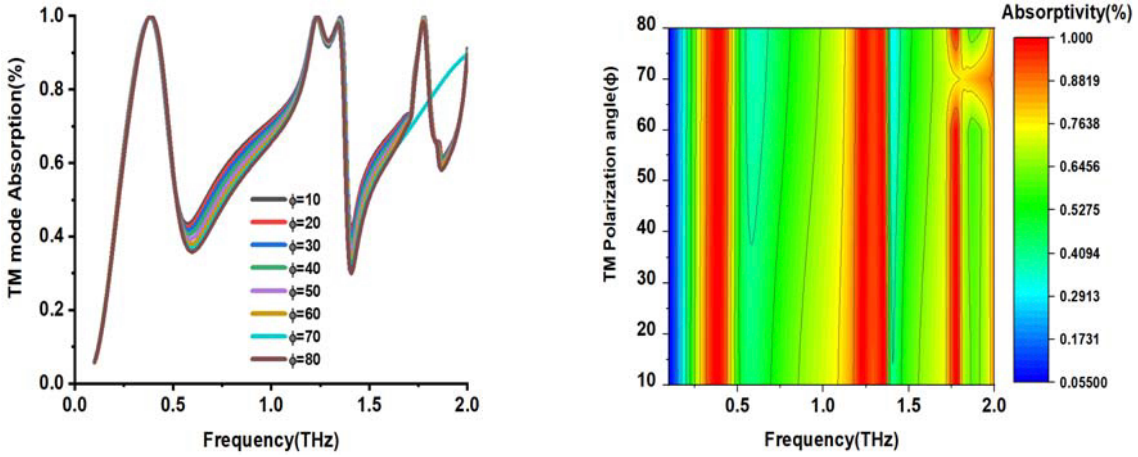

(a) (b)

Figure 11. At chemical potential (μ_c) = 0.2 eV and relaxation time (τ) = 0.2 ps, the proposed structure's absorption contour map as a function of frequency and different polarization angles (ϕ) in TM mode with (a) absorption level spectrum, (b) contour map.

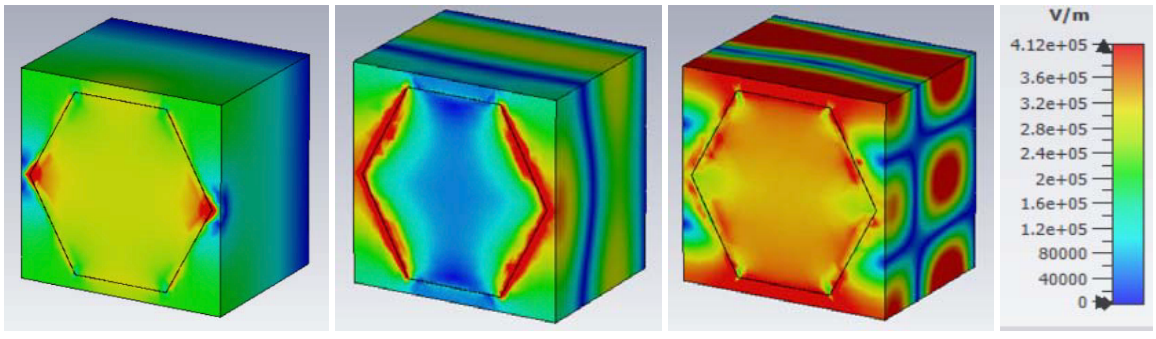

(a) (b) (c)

Figure 12. *E*-field distributions at (a) 0.386 THz, (b) 1.23 THz and (c) 1.77 THz.

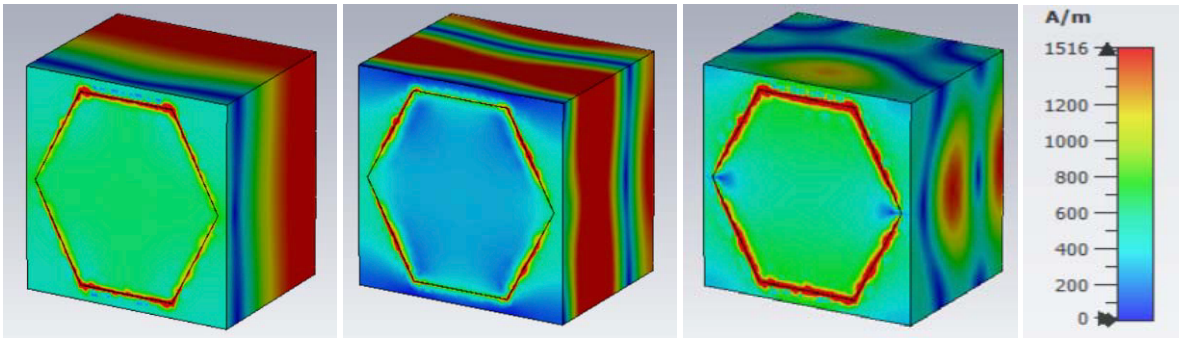

(a) (b) (c)

Figure 13. H-field distributions at (a) 0.386 THz, (b) 1.23 THz and (c) 1.77 THz.

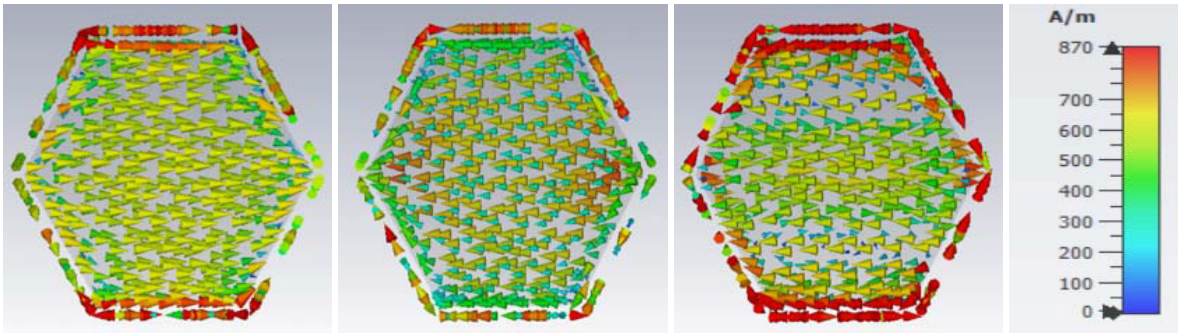

(a) (b) (c)

Figure 14. Surface current distributions on graphene patch at (a) 0.386 THz, (b) 1.23 THz and (c) 1.77 THz.

Table 1. Simulated performance comparision table of the current work with existing literature survey.

Reference	2D Unit cell size (μm^2)	Dielectric material	Absorption (%)	No of Absorption peaks	Polarization insensitive	Resonant frequencies (THz)
[2]	10×10	polymide	99.8	Single	Yes	2.2–4.6
[6]	70×55	polymide	98	Three	Yes	1.12, 2.58, 3.09
[14]	40×40	silicon	96	Two	Yes	2.44, 3.71
[17]	48.2×48.2	Sio_2	95.4, 99.9, 89.4 and 98.9	Four	Yes	1.29, 3.32, 3.85, and 4.56
[19]	73×73	-	99, 99	two	Yes	1.29, 1.61
[20]	118×118	polymide	98	Single	Yes	0.86–3.54
[21]	80×80	Silicon, Sio_2	≈ 98	Single	Yes	1.5–3.2
[22]	60×60	Silicon	≈ 96	Single	Yes	2.47–2.90
[23]	60×60	Rogers	≈ 98	Single	Yes	1.48–365
[24]	85×85	-	≈ 97	Four	Yes	0.777, 1.13, 1.53, and 2.06
[25]	80×80	Silicon, polymide	98, 96, 98	Three	Yes	0.34, 0.62 and 0.81
This work	70×70	silicon	98.6, 98.5, 99.6	Three	Yes	0.38, 1.23 and 1.77

how the proposed absorber's performance is validated using a numerical simulator. From Table 1, we can note that the proposed structure is a compact one and produces three different resonant frequencies with a percent level of absorption greater than 98.5%. Compared to the existing literature survey, the proposed structure gives good absorption and tri-bands with polarization-insensitive capability in the terahertz era, which is a notable advantage compared to the existing state of the art.

4. CONCLUSION

In this paper, we describe a polarization-insensitive metasurface absorber for terahertz applications. The overall size of the proposed structure is $70 \times 70 \times 55\,\mu m^3$, and it produces three different absorbance peaks at 0.38 THz, 1.23 THz, and 1.77 THz resonant frequencies with bandwidth ranges as 0.32 THz–0.43 THz, 1.19 THz–1.35 THz, and 1.74 THz–1.79 THz, respectively. In three absorption bands, the structure contains an absorbance level greater than 90 percent. The proposed structure possesses a polarization-insensitive nature, and the influence of different polarization angles on absorbance is verified for different modes like TE and TM. The influence of different oblique incident angles on absorbance is also described, and finally both E- and H-fields for the proposed structure are also verified as they are perpendicular to each other. Hence, it is strongly recommended that the proposed tri-band graphene-based metasurface absorber could be used for sensing, detecting applications.

REFERENCES

1. Tao, H., N. I. Landy, C. M. Bingham, X. Zhang, R. D. Averitt, and W. J. Padilla, "A metamaterial absorber for the terahertz regime: Design, fabrication and characterization," *Optics Express*, Vol. 16, No. 10, 7181–7188, 2008.
2. Zakir, S., R. M. H. Bilal, M. A. Naveed, M. A. Baqir, M. U. A. Khan, M. M. Ali, M. A. Saeed, M. Q. Mehmood, and Y. Massoud, "Polarization-insensitive, broadband, and tunable terahertz absorber using slotted-square graphene meta-rings," *IEEE Photonics Journal*, Vol. 15, No. 1, 1–8, 2022.
3. Landy, N. I., S. Sajuyigbe, J. J. Mock, D. R. Smith, and W. J. Padilla, "Perfect metamaterial absorber," *Physical Review Letters*, Vol. 100, No. 20, 207402, 2008.
4. Faruque, M. R. I., A. M. Siddiky, E. Ahamed, M. T. Islam, and S. Abdullah, "Parallel LC shaped metamaterial resonator for C and X band satellite applications with wider bandwidth," *Scientific Reports*, Vol. 11, No. 1, 1–15, 2021.
5. Ajewole, B., P. Kumar, and T. Afullo, "I-shaped metamaterial using SRR for multi-band wireless communication," *Crystals*, Vol. 12, No. 4, 559, 2022.
6. Wang, B.-X., C. Xu, G. Duan, J. Jiang, W. Xu, Z. Yang, and Y. Wu, "Miniaturized and actively tunable triple-band terahertz metamaterial absorber using an analogy I-typed resonator," *Nanoscale Research Letters*, Vol. 17, No. 1, 35, 2022.
7. Bilal, R. M. H., M. A. Baqir, P. K. Choudhury, M. Karaaslan, M. M. Ali, O. Altıntas, A. A. Rahim, E. Unal, and C. Sabah, "Wideband microwave absorber comprising metallic split-ring resonators surrounded with E-shaped fractal metamaterial," *IEEE Access*, Vol. 9, 5670–5677, 2021.
8. Li, H., J. Wang, X. Wang, Y. Feng, and Z. Sun, "Design and characterization of wideband terahertz metamaterial stop-band filter," *Micromachines*, Vol. 13, No. 7, 1034, 2022.
9. Guo, Q., Q. Peng, M. Qu, J. Su, and Z. Li, "Optical transparent metasurface for dual-band Wi-Fi shielding," *Optics Express*, Vol. 30, No. 5, 7793–7805, 2022.
10. Srilatha, K., B. T. P. Madhav, A. B. Badisa, S. Das, S. K. Patel, and J. Parmar, "Conformal and polarization adjustable cloaking metasurface utilizing graphene with low radar cross section for terahertz applications," *Optical and Quantum Electronics*, Vol. 54, No. 7, 454, 2022.
11. Dhama, R., B. Yan, C. Palego, and Z. Wang, "Super-resolution imaging by dielectric superlenses: TiO_2 metamaterial superlens versus $BaTiO_3$ superlens," *Photonics*, Vol. 8, No. 6, 222, MDPI, 2021.

12. Borhani-Kakhki, M. and T. A. Denidni, "Metamaterial enabled FSS for beam-tilting mm-Wave antenna applications," *Handbook of Metamaterial-derived Frequency Selective Surfaces*, 1–22, Springer Singapore, Singapore, 2022.
13. Yang, J. and Y.-S. Lin, "Design of tunable terahertz metamaterial sensor with single-and dual-resonance characteristic," *Nanomaterials*, Vol. 11, No. 9, 2212, 2021.
14. Li, T. Y., L. Wang, J. M. Wang, S. Li, and X. J. He, "A dual band polarization-insensitive tunable absorber based on terahertz MEMS metamaterial," *Integrated Ferroelectrics*, Vol. 151, No. 1, 157–163, 2014.
15. Al-Badri, K. S. L., A. Cinar, U. Kose, O. Ertan, and E. Ekmekci, "Monochromatic tuning of absorption strength based on angle-dependent closed-ring resonator-type metamaterial absorber," *IEEE Antennas and Wireless Propagation Letters*, Vol. 16, 1060–1063, 2016.
16. Chen, H., Z. Chen, H. Yang, L. Wen, Z. Yi, Z. Zhou, B. Dai, J. Zhang, X. Wu, and P. Wu, "Multi-mode surface plasmon resonance absorber based on dart-type single-layer graphene," *RSC Advances*, Vol. 12, No. 13, 7821–7829, 2022.
17. Jain, P., K. Prakash, G. M. Khanal, N. Sardana, S. Kumar, N. Gupta, and A. K. Singh, "Quad-band polarization sensitive terahertz metamaterial absorber using Gemini-shaped structure," *Results in Optics*, Vol. 8, 100254, 2022.
18. Asgari, S. and T. Fabritius, "Graphene-based multiband chiral metamaterial absorbers comprised of square split-ring resonator arrays with different numbers of gaps, and their equivalent circuit model," *IEEE Access*, Vol. 10, 63658–63671, 2022.
19. Feng, H., Z. Xu, K. Li, M. Wang, W. Xie, Q. Luo, B. Chen, W. Kong, and M. Yun, "Tunable polarization-independent and angle-insensitive broadband terahertz absorber with graphene metamaterials," *Optics Express*, Vol. 29, No. 5, 7158–7167, 2021.
20. Huang, X., M. Cao, D. Q. Wang, X. Li, J. Fan, and X. Li, "Broadband polarization-insensitive and oblique-incidence terahertz metamaterial absorber with multi-layered graphene," *Optical Materials Express*, Vol. 12, No. 2, 811–822, 2022.
21. Nejat, M. and N. Nozhat, "Design, theory, and circuit model of wideband, tunable and polarization-insensitive terahertz absorber based on graphene," *IEEE Transactions on Nanotechnology*, Vol. 18, 684–690, 2019.
22. Nickpay, M. R., M. Danaie, and A. Shahzadi, "A wideband and polarization-insensitive graphene-based metamaterial absorber," *Superlattices and Microstructures*, Vol. 150, 106786, 2021.
23. Norouzi-Razani, A. and P. Rezaei, "Broadband polarization insensitive and tunable terahertz metamaterial perfect absorber based on the graphene disk and square ribbon," *Micro and Nanostructures*, Vol. 163, 107153, 2022.
24. Wang, B.-X., X. Zhai, G. Z. Wang, W. Q. Huang, and L. L. Wang, "Design of a four-band and polarization-insensitive terahertz metamaterial absorber," *IEEE Photonics Journal*, Vol. 7, No. 1, 1–8, 2014.
25. Han, X., Z. Zhang, and X. Qu, "A novel miniaturized tri-band metamaterial THz absorber with angular and polarization stability," *Optik*, Vol. 228, 166086, 2021.